We are IntechOpen,
the world's leading publisher of
Open Access books
Built by scientists, for scientists

4,800
Open access books available

122,000
International authors and editors

135M
Downloads

Our authors are among the

154
Countries delivered to

TOP 1%
most cited scientists

12.2%
Contributors from top 500 universities

CLARIVATE ANALYTICS

BOOK CITATION INDEX

INDEXED

WEB OF SCIENCE™

Selection of our books indexed in the Book Citation Index
in Web of Science™ Core Collection (BKCI)

Interested in publishing with us?
Contact book.department@intechopen.com

Numbers displayed above are based on latest data collected.
For more information visit www.intechopen.com

Water Management and Experimental Diagnostics in Polymer Electrolyte Fuel Cell

Kosuke Nishida[1], Shohji Tsushima[2] and Shuichiro Hirai[2]
[1]Department of Mechanical and System Engineering, Kyoto Institute of Technology
[2]Department of Mechanical and Control Engineering, Tokyo Institute of Technology
Japan

1. Introduction

Polymer electrolyte fuel cell (PEFC) is a promising candidate for mobile and vehicle applications and distributed power systems because of its high power density and low operating temperature. However, there are several technical problems to be solved in order to achieve practicability and popularization. Especially, water management inside a PEFC is essential for high performance operation. At high current densities, excessive water generated by the electrode reaction is rapidly condensed in the cathode electrode. When the open pores in the catalyst layer (CL) and gas diffusion layer (GDL) are filled with liquid water, oxygen cannot be supplied to the reaction sites. Furthermore, water migrates significantly through the electrolyte membrane from the anode to cathode owing to electro-osmotic drag. Thus, the membrane dehydration occurs mainly on the anode side and causes the low proton conductivity during low-humidity operation. These phenomena known as "water flooding" and "dryout" are a critical barrier for high efficiency and high power density. To alleviate these issues, it is necessary to develop various diagnostic tools for understanding the fundamental phenomena of water transport between cathode and anode in PEFC.

Experimental approaches to probe water transport in PEFCs have been attempted in the previous studies. Liquid water formation, transport and removal in cathode flow channel and GDL were investigated by neutron radiography (Bellows et al., 1999; Satija et al., 2004; Kramer et al., 2005; J. Zhang et al., 2006; Turhan et al., 2006; Hickner et al., 2006; Yoshizawa et al., 2008), soft X-ray radiography (Sasabe et al., 2010), X-ray computed tomography (Lee et al., 2008), and optical visualization using transparent fuel cell (Tüber et al., 2003; Yang et al., 2004; F.Y. Zhang et al., 2006; Nishida et al., 2010a). Water content distribution in polymer electrolyte membrane (PEM) was measured by using magnetic resonance imaging (MRI) (Tsushima et al., 2004). Although various diagnostic techniques were developed as mentioned above, there are few experimental efforts to measure water distribution inside cathode GDL because of the difficulty in observing internal microstructure of opaque porous layer. Boillat et al. (Boillat et al., 2008) resolved the water distribution between the different layers of the membrane electrode assembly (MEA) in an operating PEFC using high-resolution neutron radiography. Sinha et al. (Sinha et al., 2006) have explored the possibility of using X-ray micro-tomography to quantify liquid water distribution along the

GDL thickness of a PEFC. Litster et al. (Litster et al., 2006) developed the fluorescence microscopy technique for visualizing liquid water in hydrophobic fibrous media, and applied to ex-situ measurement of water transport in a GDL. To predict two-phase flow across cathode GDL in PEFCs, numerical simulations have been also performed by many researchers. Wang et al. (Wang et al., 2001) applied a two-phase flow model based on computational fluid dynamics (CFD) to the air cathode of PEFC with a hydrophilic GDL. He et al. (He et al., 2000) and Natarajan and Nguyen (Natarajan & Nguyen, 2001) proposed two-dimensional two-phase models for PEFCs with interdigitated and conventional flow fields, respectively. Subsequently, Pasaogullari and Wang (Pasaogullari & Wang, 2004a) developed a theory describing liquid water transport in hydrophobic GDL, and explored the effect of GDL wettability on liquid water transport. Recently, Sinha and Wang (Sinha & Wang, 2007, 2008), Gostick et al. (Gostick et al., 2007) and Rebai and Prat (Rebai & Prat, 2009) have developed a pore-network model to understand the liquid water transport in a hydrophobic GDL with the GDL morphology taken into account.

This chapter introduces several novel measurement techniques for evaluating the water transport inside a PEFC (Nishida et al., 2009, 2010a, 2010b). In section 3, the experimental method for quantitatively estimating the liquid water content in the cathode gas diffusion electrode (GDE) is presented based on the weight measurement (Nishida et al., 2010a). Furthermore, the visualization tool to probe the liquid water behavior at the cathode is provided by using an optical diagnostic, and the influences of operating condition and GDL properties on the water transport through the porous electrode are discussed. Under high current density conditions, water flooding occurs significantly at the interface between cathode CL and GDL. Section 4 presents the ex-situ measurement method for evaluating the amount of liquid water accumulated at the cathode CL|GDL interface using near-infrared reflectance spectroscopy (NIRS) (Nishida et al., 2010b). NIRS is a non-invasive optical technique for quantitatively estimating the amount and concentration of water, and make it possible to determine the thickness of the liquid water film attached to the cathode CL surface after fuel cell operation. In this section, the effects of GDL hydrophobicity and microporous layer (MPL) addition on the water accumulation at the cathode CL|GDL interface are investigated. During low-humidity operation, water management on anode side is essential for achieving sufficient membrane hydration and high proton conductivity. In section 5, the imaging technique to observe the water distribution in the anode flow field of an operating PEFC is provided using water sensitive paper (WSP) (Nishida et al., 2009). WSP is a test paper for detecting water droplets, fog and high humidity. This paper is inserted into the transparent fuel cell, and makes it possible to visualize the water condensation process in the anode flow channel under low-humidity PEFC operation. To achieve better water management and alleviate membrane dryout in PEFC, the optimum operating condition is explored based on the WSP measurement. Finally, in section 6, the main conclusions derived from the present work are summarized.

2. Water transport in PEFC

Water transport in PEFC is extremely complex, and has an important impact on cell performance. Figure 1 schematically shows a cross-sectional view of PEFC and its water transport processes. A PEM film coated with CLs on both sides is sandwiched between two hydrophobic GDLs. Hydrogen and oxygen as fuel and oxidant are supplied to the anode

and cathode sides, respectively. Hydrogen gas diffuses through the anode GDL to the active reaction sites inside the CL. At the anode CL, hydrogen dissociates into protons (H^+) and electrons. Protons migrate through the electrolyte membrane to the cathode electrode. On the cathode side, protons combine with electrons and oxygen, and produce water. The external flow of electrons can be utilized for electric power. At high current operations, excessive water is generated in the cathode CL. A small part of the product water is reversely diffused through the membrane from the cathode to anode, and the electrolyte membrane is hydrated. On the other hand, most of the product water is condensed and accumulated inside the cathode CL and GDL. If open pores in the CL and GDL are filled with liquid water, or if the gas channels are clogged by liquid water, oxygen transport to the reaction sites is hindered. These phenomena known as "water flooding" and "plugging" are an important limiting factor for PEFC performance. Furthermore, water is transported from the anode to cathode in the PEM by electro-osmotic effect. Thus, under low-humidity conditions, the membrane dehydration proceeds mainly on the anode side and the proton conductivity declines. This anode dryout causes a substantial drop in cell voltage, resulting in not only temporary power loss but also cell degradation. In operating PEFC, transversal water distribution in MEA is complicatedly determined as a result of coupled processes including water generation, evaporation, condensation, back-diffusion, electro-osmotic and interfacial mass transfer. To achieve proper water management and improve cell performance, it is necessary to obtain the fundamental understandings of water transport inside fuel cell.
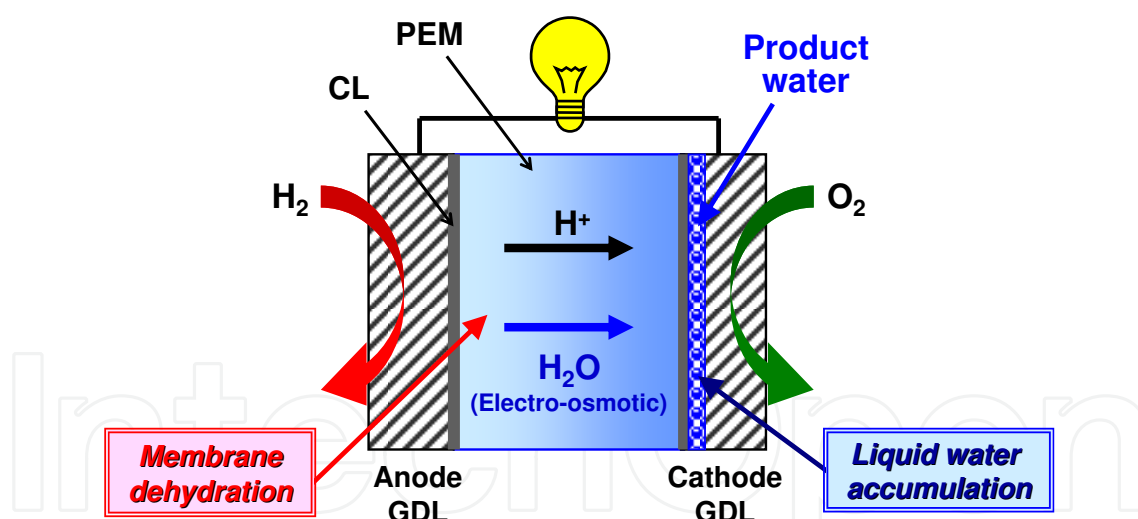

Fig. 1. Cross-sectional view of PEFC and its water transport processes

3. Measurement of liquid water content in cathode gas diffusion electrode

This section presents a novel method for quantitatively estimating the average liquid water content inside the cathode gas diffusion electrode (GDE) of a PEFC based on the weight measurement (Nishida et al., 2010a). In addition, the liquid water behavior at the cathode during cell operation is visualized using an optical diagnostic, and the influences of current density and GDL thickness on the water transport through the cathode GDE are also discussed.

3.1 Estimation method for liquid water content in cathode GDE

By measuring the weights of liquid water accumulated in the MEA and PEM, the average liquid water content in the cathode GDE of an operating cell can be predicted. The cathode GDE structurally consists of a cathode GDL and CL. In this experiment, the time-series data of cell voltage is also monitored during cell operation to investigate the relationship between the water accumulation in the cathode GDE and the voltage change. However, the evaluation of liquid water content in the GDE and the sequential monitor of cell voltage are conducted at difference times, because the assembled cell must be composed in measuring the weight of liquid water in the MEA.

The average liquid water content in the cathode GDE, X_W, is defined as the averaged volume fraction of liquid water in the porous media, and given by

$$X_W = \frac{(\Delta m_{MEA} - \Delta m_{PEM}) \cdot v_W}{V_{GDL}} \times 100 \tag{1}$$

where Δm_{MEA} and Δm_{PEM} are the weight increases of the MEA and PEM due to the liquid water generation, respectively. v_W denotes the specific volume of liquid water, and V_{GDL} the pore volume inside the cathode GDL. The MEA used in this experiment is constructed of a PEM film and two GDEs including CL. In this estimation, the liquid water volume in the CLs is neglected because the thickness of CL is very thin and the pore volume is extremely small. Furthermore, since dry hydrogen is supplied to the anode side without humidification, the water condensation in the anode GDE hardly occurs. The water influx to the anode is only due to the back diffusion through the membrane. Therefore, the liquid water accumulation in the anode GDE can be also ignored. Under these assumption, the average liquid water content in the cathode GDE including the CL is described by Equation (1). Δm_{MEA} is given by measuring the weights of the MEA experimentally before and after operation test.

The weight of the PEM, m_{PEM}, in Equation (1) is estimated by

$$m_{PEM} = m_{dry} \left(\frac{18\lambda}{EW} + 1 \right) \tag{2}$$

where m_{dry} is the weight of the dry membrane, λ the water content in the membrane, and EW the equivalent weight of the dry membrane. The water content, λ, is calculated by

$$\lambda = \frac{\sigma}{0.005139} \exp \left[1268 \left(\frac{1}{273 + T} - \frac{1}{303} \right) \right] + 0.63436 \tag{3}$$

where σ is the membrane conductivity and T is the cell temperature. This equation was empirically obtained from measuring the membrane water content and conductivity under a range of water vapor activities at 30ºC (Springer et al., 2005). The membrane conductivity, σ, is also given by Equation (4)

$$\sigma = \frac{t_{PEM}}{R_{PEM} \cdot A} \tag{4}$$

where t_{PEM} is the membrane thickness, R_{PEM} the membrane resistance, and A the electrode reaction area. R_{PEM} is measured by using AC impedance method.

3.2 Experimental

Figure 2 shows the experimental setup used for PEFC operation test, which consists of a constant temperature chamber, a gas supply unit, a high-resolution digital CCD camera, a transparent fuel cell, an electronic load, a data logger, and a personal computer. To directly observe the liquid water behavior at the cathode electrode, a quartz glass is inserted into the experimental fuel cell as a window. The experimental cell equipped with the transparent window is operated in the constant temperature chamber in order to maintain the cell temperature. The digital CCD camera with the zoom lens for optical visualization is set outside of the constant temperature chamber, and the working distance from the cathode electrode of the transparent fuel cell is adjusted. The cathode flow field is illuminated by a halogen light source and the close-up images of the GDL surface can be clearly captured. The time-series output voltage and temperature of the operating fuel cell are recorded by the data logger. The cell temperature is measured using a thermocouple. The high frequency resistance (HFR) of the PEM is also measured by the LCR meter.
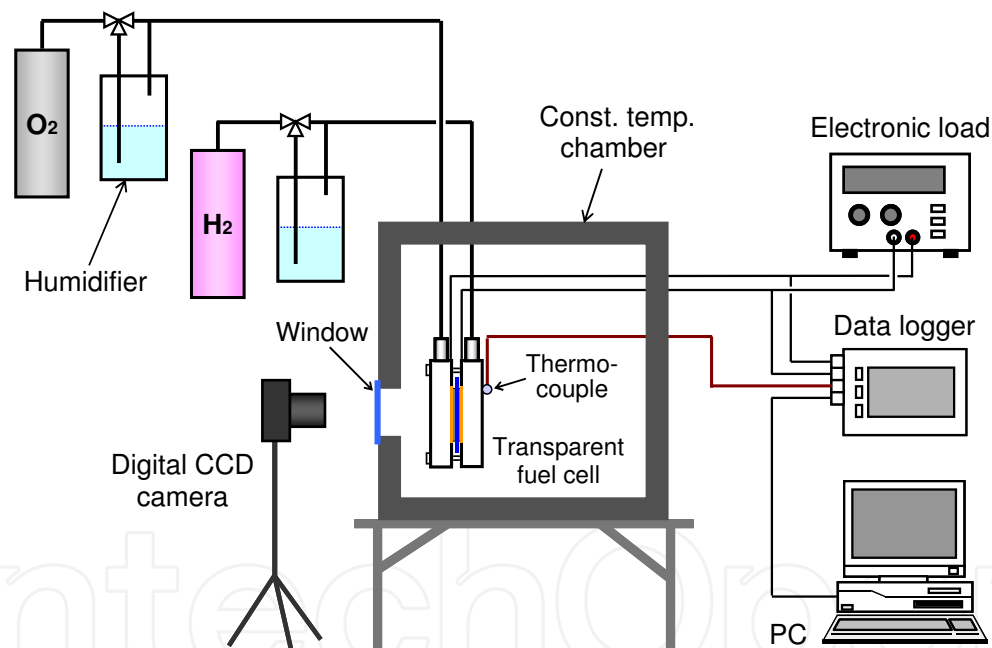

Fig. 2. Experimental setup used for PEFC operation test

The schematic diagram and photograph of the transparent fuel cell are shown in Figure 3. The catalyst coated membrane (CCM) on which Pt particles are loaded is sandwiched between two PTFE-proofed GDLs. In addition, the MEA constructed of the PEM, two CLs and two GDLs is sandwiched between two copper current collector plates with gold coating. The active area of the experimental cell used in this study is 5 cm². Two stainless steel separators which have a single-pass serpentine flow channel are placed outside the current collectors and held together by four M6 bolts. The width, depth and overall length of the serpentine channel are 2 mm, 2 mm, and 10.5 cm, respectively. In this experiment, dry hydrogen and oxygen are fed into the anode and cathode channels at constant flow rates without humidification.
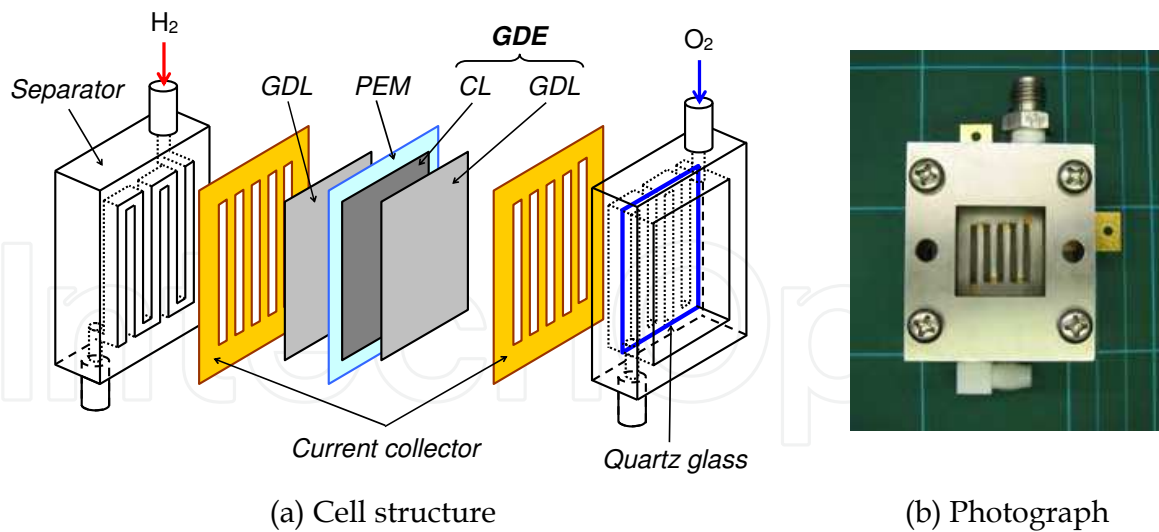
(a) Cell structure   (b) Photograph

Fig. 3. Shematic diagram and photograph of the transparent fuel cell

Figure 4 shows the experimental procedure for estimating the liquid water content in the cathode GDE. Beforehand, the weight of the dry MEA is measured by an electronic balance. Furthermore, the HFR of the electrolyte membrane is also measured by the LCR meter, and the water content in the PEM is predicted. Subsequently, the pre-operation of the experimental fuel cell is carried out at 0.16 A/cm² for 2 hours in order to hydrate the
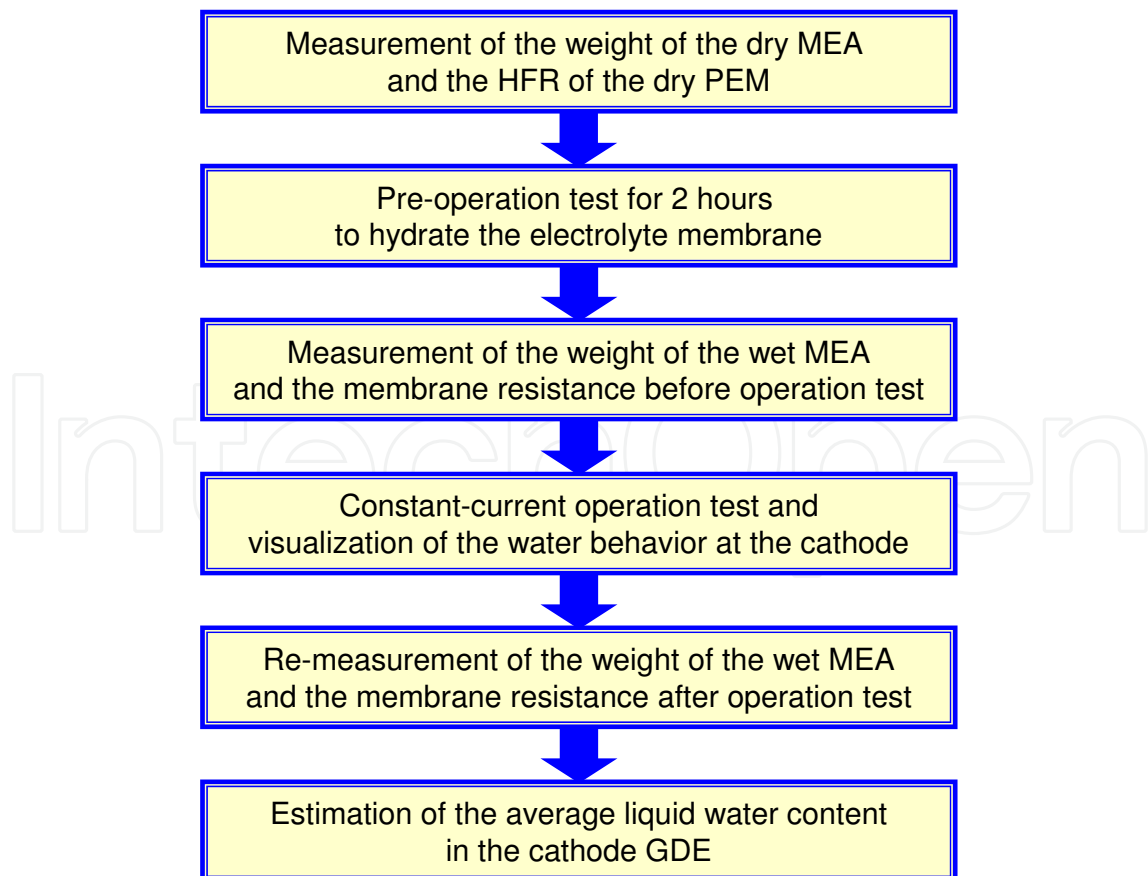
Fig. 4. Experimental procedure for estimating the liquid water content in the cathode GDE

electrolyte membrane. After the pre-operation, the assembled fuel cell is decomposed into the MEA, current collectors and separators, and the weight of the wet MEA and the membrane resistance are measured. The adherent liquid droplets on the GDL surface are wiped away before the measurement. Then the MEA is slowly dried until the liquid water weight in the cathode GDE is adjusted to the initial state. The liquid water weight in the cathode GDE is given by subtracting Δm_{PEM} from Δm_{MEA}. Following the membrane hydration, the constant-current operation test is conducted, and the liquid water behavior at the cathode is directly visualized by using the digital CCD camera. The cell voltage during operation is also monitored. Finally, after the operation test, the experimental cell is decomposed and the weight of the wiped MEA and the membrane resistance are measured again. The average liquid water content in the cathode GDE is quantitatively evaluated by Equation (1).

In order to investigate the relationship between the water content in the cathode GDE and the operation time, the operation test and the estimation of water content need to be repeated again and again because the assembled cell must be decomposed in measuring the weight of water in the MEA.
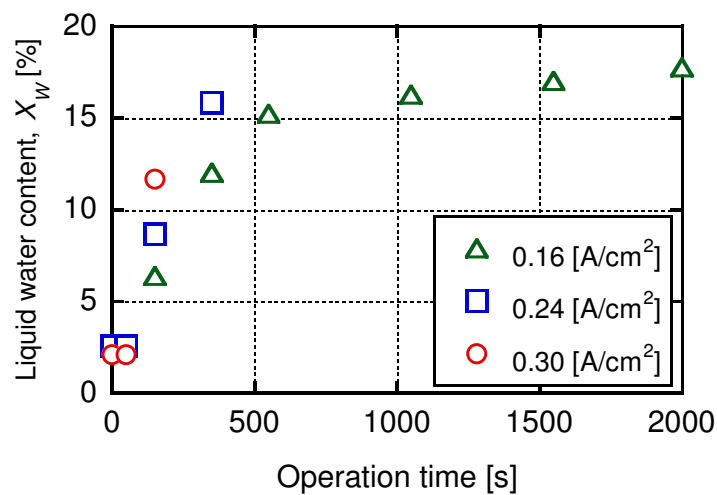
3.3 Cell voltage vs. liquid water content in cathode GDE

PEFC performance is largely influenced by liquid water accumulation in cathode GDL and CL. The characteristics of the cell voltage and the average liquid water content in the cathode GDE are shown in Figure 5. The GDL used for this experiment is Toray TGP-H-120 carbon paper (360 μm thick). The current density as an operating parameter is set to 0.16, 0.24 and 0.3 A/cm². In all experiments, the fuel cell is held under the open circuit condition for the first 50 s. Figure 5(a) presents the voltage change during startup operation at 20°C. At the low current density of 0.16 A/cm², the fuel cell operates stably for 2000 s though the cell voltage decreases a little. When the current density increases up to 0.3 A/cm², the sudden voltage drop occurs immediately after starting the operation.

The relationships between the average liquid water content in the cathode GDE and the operation time are plotted in Figure 5(b). Since the assembled cell must be decomposed in measuring the weight of liquid water in the MEA, these plots were obtained from many different operation tests. In the case of 0.16 A/cm², the liquid water content in the cathode GDE increases rapidly up to approximately 15% for 500 s after starting the operation. After t=500 s, the rate of increase of the water content slows down because the liquid water accumulated in the GDL is drained to the flow channel. When the current density increases, the rate of increase of the water content in the GDE increases due to the production of much water. In the case of 0.24 and 0.3 A/cm², the cell voltages reduce to zero at t=400 and 200 s, though the water contents reach only 16 and 12%, respectively. It can be considered that the oxygen transport through the GDL is not limited because of low water content. Therefore, these sudden voltage drops are probably due to the mass transfer limitation within the CL. If most of the cathode CL is covered with the condensed water, oxygen cannot be sufficiently supplied to the reaction sites and the concentration overpotential is remarkably increased. The amount of liquid water accumulated in the CL tends to increase with an increase in current density.
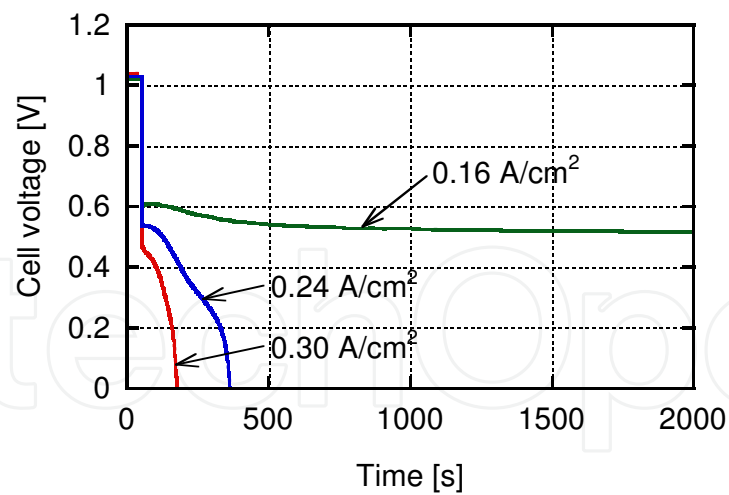
(a) Cell voltage

(b) Water content in cathode GDE

Fig. 5. Comparison of the cell voltage and average liquid water content in the cathode GDE at 0.16, 0.24 and 0.3 A/cm²

3.4 Visualization image of liquid water behavior at cathode

Figure 6 shows the sequential images of liquid water behavior on the cathode GDL at the current density of 0.16 A/cm². The cathode gas flows from the upper right to the lower left in the serpentine flow field which has five straight channels. Liquid water is hardly drained from the cathode GDE for 300 s after starting the operation. However, a few liquid droplets accumulated in the cathode GDE appear on the electrode surface at t=500 s. These droplets on the GDL surface grow and the number of water droplets increases after 500 s of operation. It is noted that the gradual increase of the water content in the cathode GDE after t=500 s shown in Figure 5(b) is due to the liquid water removal from the GDE.

3.5 Effect of GDL thickness on liquid water accumulation in cathode GDE

Liquid water transport in cathode GDE is also affected by thickness and porous structure of GDL. Figure 7 presents the effect of GDL thickness on the cell voltage and liquid water

Fig. 6. Visualization images of liquid water behavior on the cathode GDL at 0.16 A/cm²

accumulation in the cathode GDE at 0.24 A/cm². In this experiment, two different thickness paper-type GDLs of Toray TGP-H-060 and TGP-H-120 are used. The properties of these GDLs are described in Table 1. The thickness of TGP-H-060 is approximately half of that of TGP-H-120. Figure 7(a) shows the voltage changes for two different GDLs during startup at 20ºC. In the case of thick GDL (TGP-H-120), the cell voltage drops suddenly after starting the fuel cell operation. On the other hand, the cell voltage for the thin GDL (TGP-H-060) case remains constant for 8000 s, because liquid water in the cathode CL and GDL is smoothly removed and oxygen is stably supplied to the reaction sites.

|	TGP-H-060	TGP-H-120
Type	Carbon paper	Carbon paper
Thickness	190 μm	360 μm
Porosity	0.78	0.78

Table 1. Properties of GDLs

The weights of liquid water accumulated in the cathode GDE in both cases are plotted in Figure 7(b). The rate of the water accumulation for the thin GDL (TGP-H-060) is slower than that for the thick GDL (TGP-H-120). This is because the liquid water inside cathode GDE is quickly drained to the flow channel after starting the operation in the case of thin GDL. In the case of thick GDL, the cell voltage decreases to zero at t=400 s though the weight of liquid water in the GDE reaches only 21 mg. The weight of water of 21 mg is equivalent to

the low water volume fraction of 15.8% in the GDE. This result indicates that most of the product water tends to remain inside the cathode CL in the case of thick GDL.
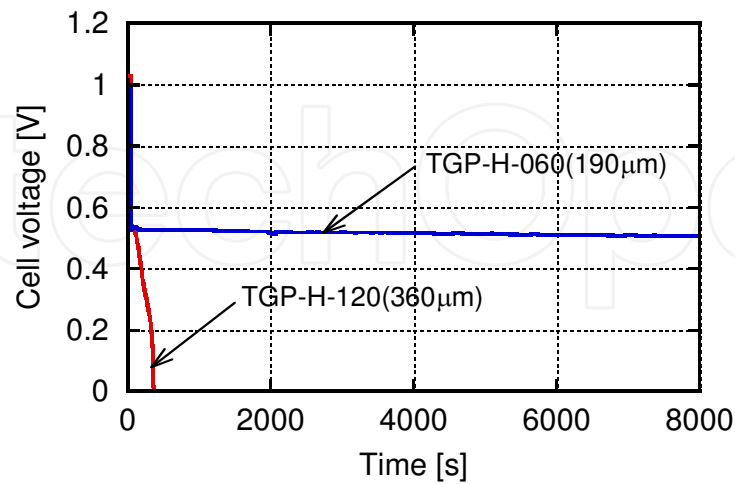
(a) Cell voltage
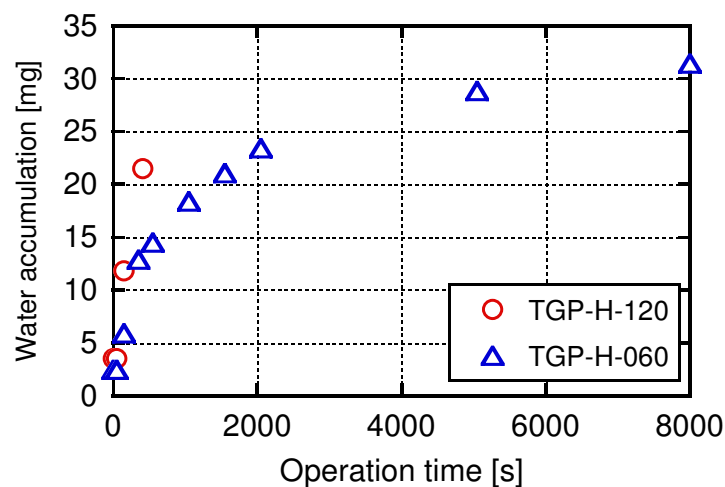
(b) Water accumulation in cathode GDE

Fig. 7. Effect of GDL thickness on the cell voltage and liquid water accumulation in the cathode GDE at 0.24 A/cm²

4. Quantitative evaluation of liquid water at cathode CL|GDL interface using near-infrared reflectance spectroscopy

The significant performance loss at high current densities is attribute to severe oxygen transport limitation inccured by water flooding at the interface between cathode CL and GDL. This section presents a diagnostic method for quantitatively evaluating the amount of liquid water accumulated at cathode CL|GDL interface of a PEFC using near-infrared reflectance spectroscopy (NIRS) (Nishida et al., 2010b). In this measurement, the effects of GDL hydrophobicity and MPL addition on the water accumulation at the CL|GDL interface are investigated.

4.1 Near-infrared reflectance spectroscopy (NIRS)

Near-infrared reflectance spectroscopy (NIRS) is an absorption spectroscopy technique for quantitatively estimating the amount of water based on Lambert-Beer's law. Figure 8 shows the fiber-optic NIRS measurement system used in this study. This NIRS system consists of a tungsten light source, optical filter, optical fiber, PbS detector, sampling circuit and analog computing circuit. The incident light emitted from the tungsten light source is separated into the measuring light (wavelength: λ_1=1.94 μm) and two reference lights (wavelength: λ_2, λ_3=1.8, 2.1 μm) by the optical filter. Each light passes through the optical fiber and illuminates the cathode CL surface of the catalyst coated membrane (CCM) removed from a PEFC. The reflected lights from the CL surface are conducted along the optic cable to the PbS detector and converted the electrical signals. The output value, α, from the NIRS system is expressed by Equation (5)

$$\alpha = K \cdot \log \frac{E_2 + E_3}{2E_1} \tag{5}$$

where K is gain constant. E_1, E_2 and E_3 are the energies of the measuring light and two reference lights, respectively. Since the reference lights are also received by the detector, the impacts of light collection efficiency and environmental changes on the measurement results can be neglected. When the measuring light travels through the liquid water film attached to the CL surface, the light intensity decreases exponentially. The thickness of the water film at the cathode CL|GDL interface is quantitatively obtained from the absorbance of the measuring light.
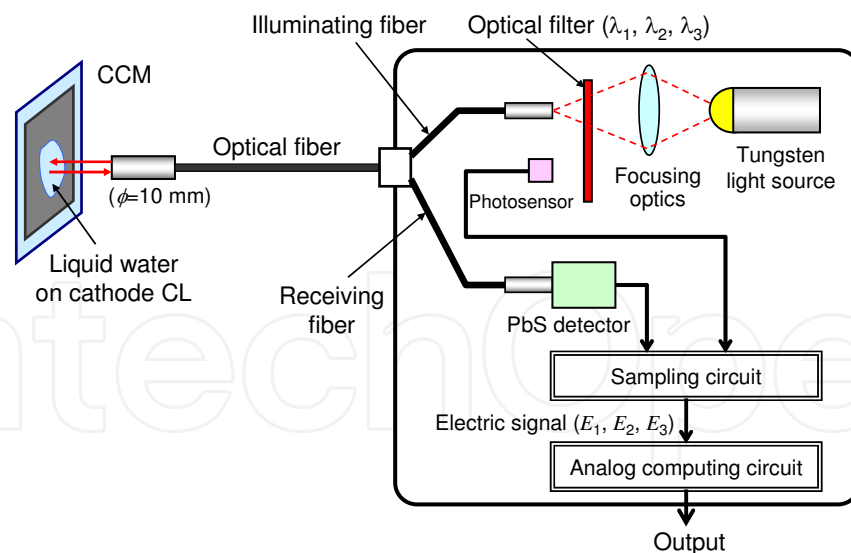

Fig. 8. Fiber-optic NIRS measurement system

For near-infrared (NIR) absorption spectroscopy of liquid water, it is essential to select a strong absorption band. Figure 9 presents the absorption coefficients of liquid water at 20ºC in the wavelength range from 0.7 to 2.5 μm (Curcio & Petty, 1951). There are five prominent water absorption bands in the NIR which occur at 0.76, 0.97, 1.19, 1.45 and 1.94 μm. In the NIRS system, the maximum absorption band at 1.94 μm is used for the measuring light.
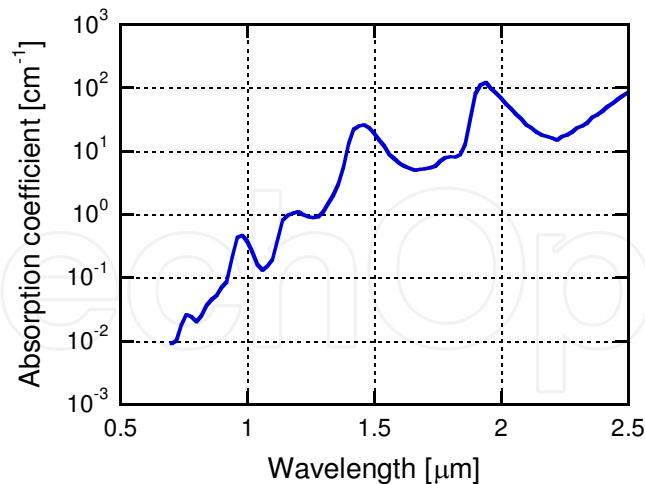
Fig. 9. Absorption coefficients of liquid water at 20°C in the wavelength range of 0.7-2.5 µm (Curcio & Petty, 1951)

4.2 Experimental

The calibration must be carried out beforehand to obtain the amount of liquid water attached to the cathode CL from the absorbance of the NIR light. To establish the calibration curve, the liquid water accumulation on the cathode CL surface is quantitatively estimate by the weight measurement. The average thickness of liquid water film on the CL surface, t (µm), is calculated by Equation (6)

$$t = \frac{w_{wet} - w_{dry} - w_{liq}}{\rho A} \times 10^4 \tag{6}$$

where w_{wet} is the weight (g) of the CCM with a wet cathode surface, w_{dry} is the weight (g) of the dry CCM, w_{liq} the weight (g) of liquid water that penetrates into the CCM, ρ the density of liquid water (g/cm³), and A the electrode area (cm²). Figure 10 presents the calibration curve for the conversion of the measurement value, α to the average thickness of liquid water on the CL surface. The calibration curve is formulated as

$$\alpha = -0.095216t^2 + 8.0483t + 871.27 \tag{7}$$

The structure of the experimental fuel cell used in this measurement is the same as that in Figure 3. The CCM on which platinum particles (0.5 mg/cm²) are loaded as a catalyst layer is sandwiched between two PTFE-proofed paper-type GDLs (Toray TGP-H-060). After cell operation, the wet CCM is removed from the assembled cell, and the amount of liquid water on the cathode CL surface is measured using the fiber-optic NIRS system. Figure 11 shows four measurement positions of NIRS on the cathode CL surface of the CCM. The cathode gas flows from the upper right to the lower left through the serpentine channel. Thus, position (1) and (2) are located in the upstream section of the cathode flow field, and (3) and (4) are located in the downstream.
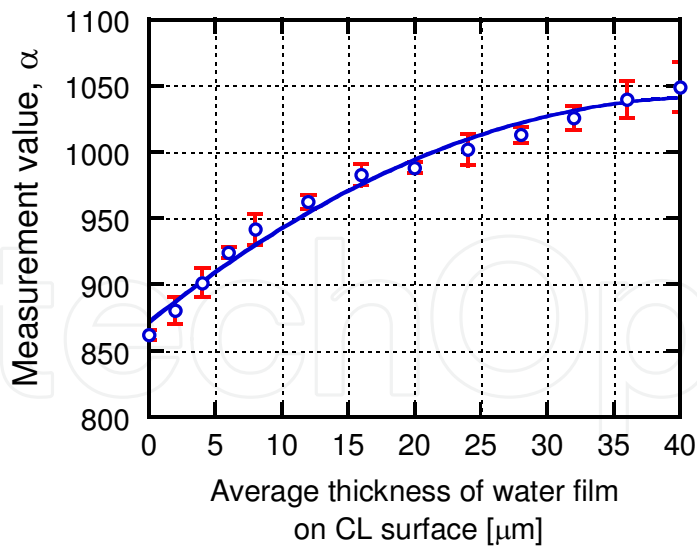
Fig. 10. Calibration curve for the conversion of the measurement value, α to the average thickness of liquid water on the CL surface
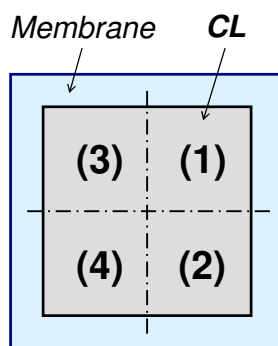
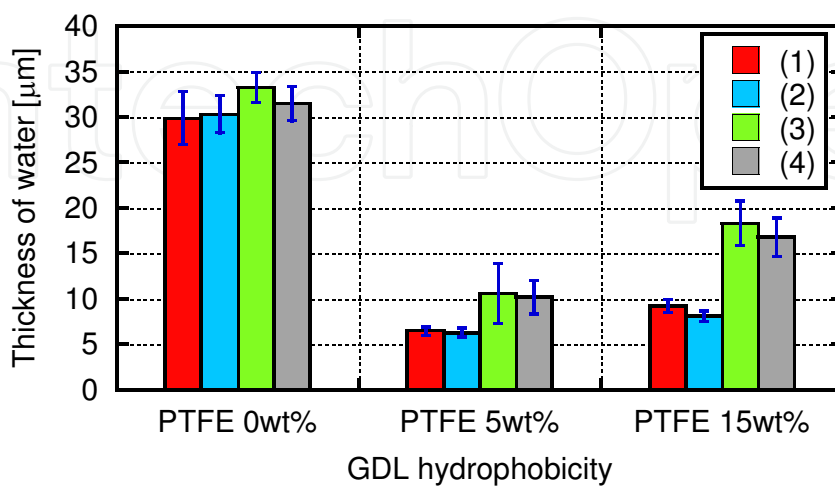Fig. 11. Measurement positions of the fiber-optic NIRS system on the cathode CL surface

Fig. 12. Effect of GDL hydrophobicity on liquid water accumulation on the cathode CL surface

4.3 Effect of GDL hydrophobicity on water transport at cathode CL|GDL interface

Liquid water accumulation at cathode CL|GDL interface is largely affected by GDL hydrophobicity. In this subsection, the effect of PTFE content of GDL on the water accumulation at the cathode interface is investigated. Figure 12 presents the thickness of liquid water film attached to the cathode CL surface for hydrophilic (PTFE content: 0 wt%) and hydrophobic (5 and 15 wt%) GDLs. The water measurements in both cases were carried out using the fiber-optic NIRS system shown in Figure 8 after fuel cell operation. The experimental fuel cell is operated at 20°C and 0.3 A/cm² for 60 min. In each case, many operation tests were repeated to confirm the reproducibility of the NIRS results. Each bar graph was obtained by averaging several experimental data, and the error bars were provided. (1), (2), (3) and (4) denote the NIRS measurement positions shown in Figure 11. In the case of hydrophilic GDL (0 wt% PTFE), the thickness of water film reaches more than 30 μm in all positions in spite of the short operation time. When the thickness of liquid film accumulated at the cathode CL|GDL interface increases beyond 30 μm, oxygen gas cannot be sufficiently supplied to the reaction sites, and the fuel cell operates unstably. The amount of adherent water for the hydrophobic GDLs (5 and 15 wt% PTFE) is much less than that for the hydrophilic GDL. The hydrophobic treatment of GDL is effective in alleviating liquid water accumulation at cathode CL|GDL interface. However, the thickness of water film on the CL surface at 15 wt% PTFE is thicker than that at 5 wt%. This is probably because the highly hydrophobic treatment of GDL blocks the inflow of liquid water into the porous GDL.

4.4 Effect of MPL addition on water transport at CL|GDL interface

It is well known that microporous layer (MPL) placed between CL and GDL reduces the negative effect of water flooding at cathode (Pasaogullari & Wang, 2004b; Nam & Kaviany, 2003; Nam et al., 2003). MPL consisting of carbon black and PTFE is coated on one side of a coarse GDL, and has micro-structural and highly hydrophobic characteristics. In subsection 4.4, the influence of MPL addition on the liquid water accumulation at the interface between the cathode CL and MPL is investigated using the NIRS measurement. Table 2 presents the thickness of water film on the cathode CL in the cases without and with MPL. The amounts of carbon black and PTFE in the MPL are 2.0 mg/cm² and 2.0 mg/cm², respectively. The NIRS measurements in both cases were conducted after 60 min of operation. The current density and PTFE content for GDL are 0.3 A/cm² and 15 wt%. It is noted that the liquid water film on the cathode CL is not formed at all by the MPL addition.

Figure 13 shows the schematic diagram of water transport mechanisms at cathode CL|GDL interface without and with MPL. In the case without MPL, micro-scale liquid droplets attached to the cathode CL grow up and fill the large pores of GDL. The formation of liquid water film at the cathode CL|GDL interface is governed by the coarse pore structure of GDL. On the other hand, small pores in the MPL prevent the interfacial water droplets at the CL|MPL interface from growing large, and reduce the water saturation level. The fine pore structure of MPL is effective in preventing water flooding at cathode CL|MPL interface.

	(1)	(2)	(3)	(4)
Without MPL	9.2 μm	8.1 μm	18.4 μm	16.8 μm
With MPL	0.1 μm	0.0 μm	0.1 μm	0.0 μm

Table 2. Effect of MPL addition on the thickness of water film on the cathode CL surface
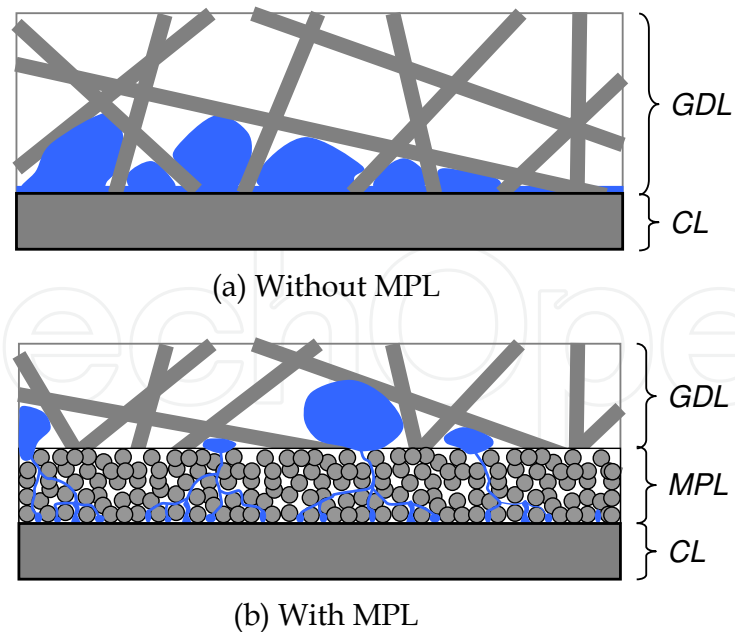
(a) Without MPL

(b) With MPL

Fig. 13. Schematics of liquid water transport at the cathode CL|GDL interface without and with MPL

5. Measurement of water distribution in anode flow field under low-humidity conditions

In operating PEFCs, water migrates through electrolyte membrane from anode side to cathode side due to electro-osmotic effect. Thus, membrane dehydration occurs mainly near anode inlet under low-humidity conditions. In this section, the water vapor condensation in a PEFC is optically visualized by using water sensitive paper (WSP), and the water distribution in the anode flow field is investigated during low-humidity operation (Nishida et al., 2009).

5.1 Water sensitive paper

In order to visualize the water condensation in the anode flow field of an operating fuel cell, water sensitive paper (WSP), which is a test paper for water detection manufactured by Syngenta, was used in this experiment. Figure 14 shows the photograph of WSP sheet. The thickness of WSP is approximately 100 μm. WSP is coated with a yellow surface, which is changed into dark blue when exposed to water droplets, fog and high humidity. Figure 15
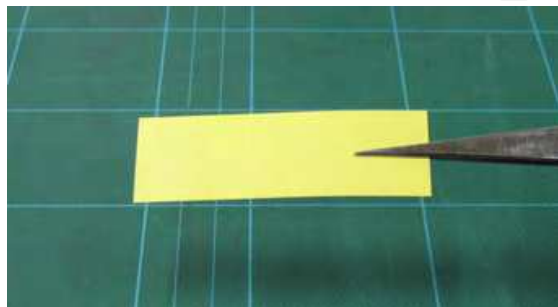

Fig. 14. Photograph of water sensitive paper (WSP)

presents the discoloration images of WSP when exposed to three different high humidity environments (RH=60, 70 and 80%) at 70ₒC. At the relative humidity of 60%, the surface color of WSP is hardly changed for 1000 s. On the other hand, when the relative humidity increases up to 70%, the yellow surface of WSP discolors to blue at t=500 s. The discoloration of WSP proceeds quickly when the environmental relative humidity reaches more than 80%.

5.2 Experimental

To directly observe the discoloration image of WSP in the anode flow channel, the experimental equipment and transparent fuel cell shown in Figure 2 and 3 are used. For water measurement, three sheets of WSP (1.0 mm x 30 mm) are inserted between the anode GDL and current collector, and a quartz glass is installed in the anode end plate as a window. The photo image of the anode flow field with three WSP sheets in the transparent cell is shown in Figure 16. Pure hydrogen and oxygen as the fuel and oxidant are fed into the anode and cathode channels at RH=0 or 30%. The utilization of hydrogen and oxygen are 0.4 and 0.2, respectively. The cell temperature in this experiment is set to 70ₒC.

| 100 s | 200 s | 500 s | 1000 s |

(a) RH=60%

| 100 s | 200 s | 500 s | 1000 s |

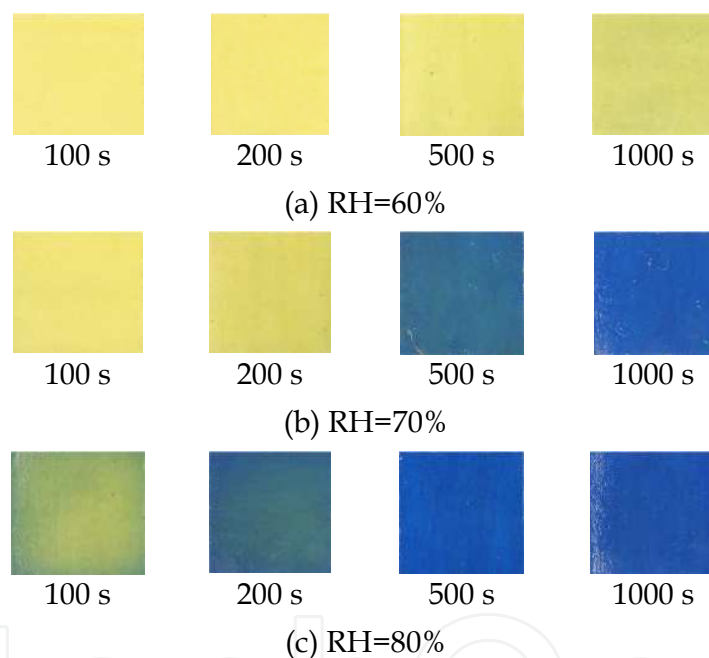(b) RH=70%

| 100 s | 200 s | 500 s | 1000 s |

(c) RH=80%

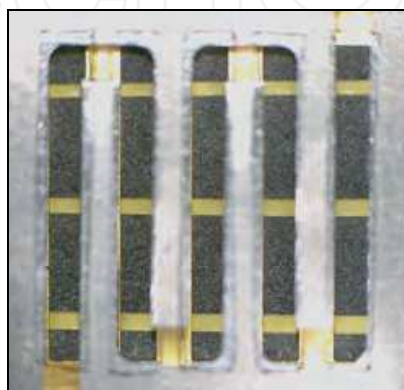Fig. 15. Discoloration images of WSP when exposed to high humidity environments at 70ₒC

Fig. 16. Photo image of the anode flow field with three WSP sheets in the transparent fuel cell

5.3 Water distribution in anode flow field for operation without humidification

Figure 17 shows the time-sequential images of the WSP discoloration in the anode flow field under non-humidity condition. The operation test was conducted at 70°C and 0.1 A/cm². The gas streams along the anode and cathode channels are arranged in co-flow. The anode gas (dry H_2) flows from the upper right to the lower left in the serpentine flow channel. The WSP surface begins to discolor from yellow to blue in the downstream section of the anode channel at t=100 s. This result suggests that the product water on the cathode side is reversely diffused toward the anode through the electrolyte membrane. Water concentration profile in anode channel during non-humidity operation is dominated by water generation at cathode and back-diffusion of water in electrolyte membrane. As seen in the photograph, the anode water condensation occurs gradually from the downstream section after startup, because of the strong back-diffusion of water from the cathode downstream.
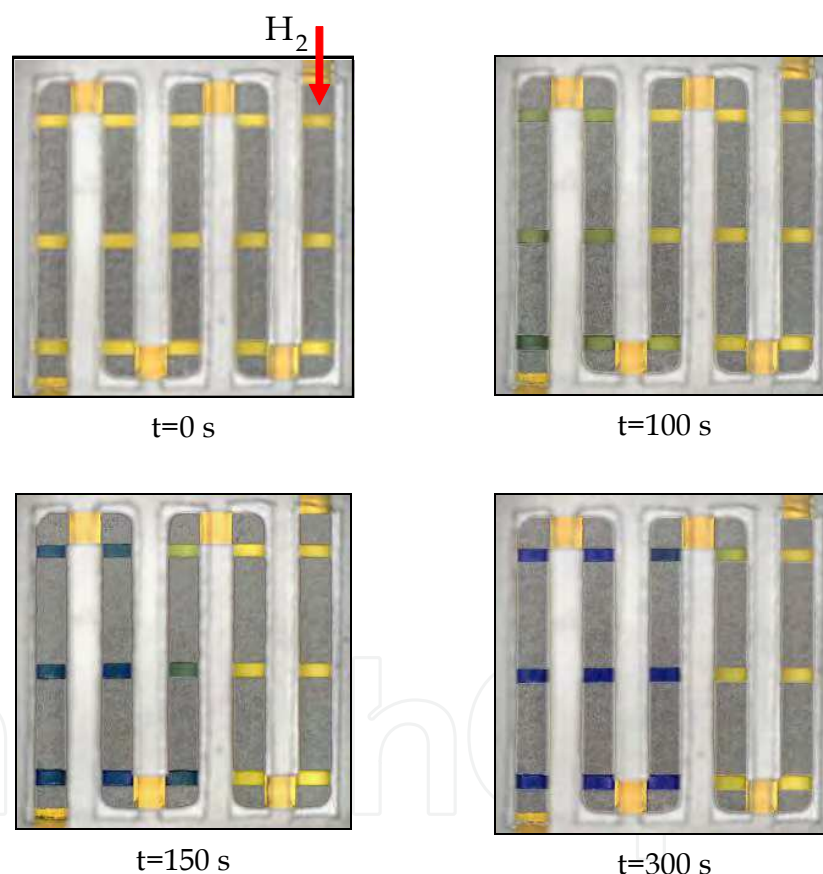

Fig. 17. Visualization images of the WSP discoloration in the anode channel under non-humidity condition at 0.1 A/cm²

5.4 Effect of inlet gas humidification on anode water distribution and cell performance

In this subsection, the influence of inlet gas humidification on the anode water distribution and the proton conductivity of the electrolyte membrane is discussed under low and high current densities.

5.4.1 Low current density operation

Figure 18 presents the discoloration images of WSP in the anode flow channel taken after 1000 s of operation at two different humidification conditions. In this experiment, either anode or cathode inlet gas is humidified to 30% RH. The experimental fuel cell is operated at the low current density of 0.1 A/cm². The anode gas flows from the upper right to the lower left in both images. In both cases of A/C=30/0 and 0/30%, the WSP sheets positioned from the second to fifth channel are changed into dark blue by the inlet humidification and water back-diffusion. Under low current conditions, the water distribution in the anode flow field for the anode humidification case (A/C=30/0%) is almost similar to that for the cathode humidification (A/C=0/30%).

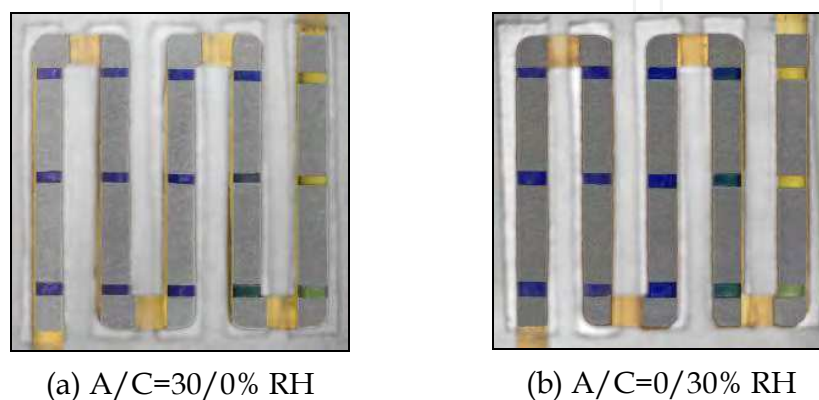(a) A/C=30/0% RH   (b) A/C=0/30% RH

Fig. 18. Discoloration images of WSP in the anode channel for two different humidification conditions (Anode/Cathode(A/C)=30/0%, 0/30% RH) at low current density of 0.1 A/cm²
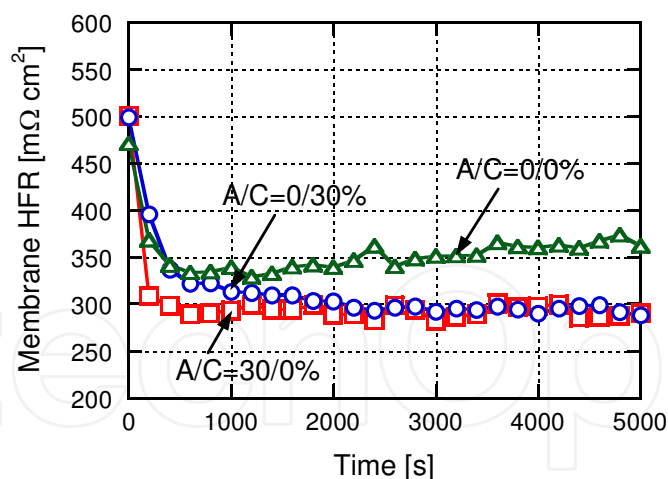

Fig. 19. Membrane HFRs for different humidification conditions (A/C=0/0%, 30/0%, 0/30% RH) at low current density of 0.1 A/cm²

Figure 19 shows the high frequency resistance (HFR) of the electrolyte membrane during cell operation at three humidification conditions (A/C=0/0, 30/0 and 0/30% RH). The humidification of anode or cathode inlet is effective in reducing the membrane resistance and improving the cell performance because of encouraging the membrane hydration. The membrane HFR in the anode humidification case is almost same as that in the cathode humidification.

5.4.2 High current density operation

During low-humidity operation at high current densities, much water is significantly transported through electrolyte membrane from anode to cathode by strong electro-osmotic effect. Figure 20 presetns the discoloration images of WSP in the anode flow channel at the high current density of 0.3 A/cm². The inlet humidification condition is A/C=30/0 and 0/30% RH. Each picture was taken after 1000 s of operation. As seen in the photograph, the anode water concentration at 0.3 A/cm² is lower than that at 0.1 A/cm² shown in Figure 18. The decrease of the water concentration on the anode side is due to the strong water transport to the cathode driven by electro-osmotic drag. In the case of cathode humidification (A/C=0/30%), the WSP sheets positioned in only the fifth channel are changed into blue by the back-diffusion of water. On the other hand, when the anode inlet is humidified to 30%, the discoloration area of WSP in the anode flow field is expanded from the fifth to fourth channel. Under high current density condition, water shortage occurs mainly on anode side owing to electro-osmotic effect. Therefore, anode inlet humidification is effective in increasing water concentration in anode flow channel.
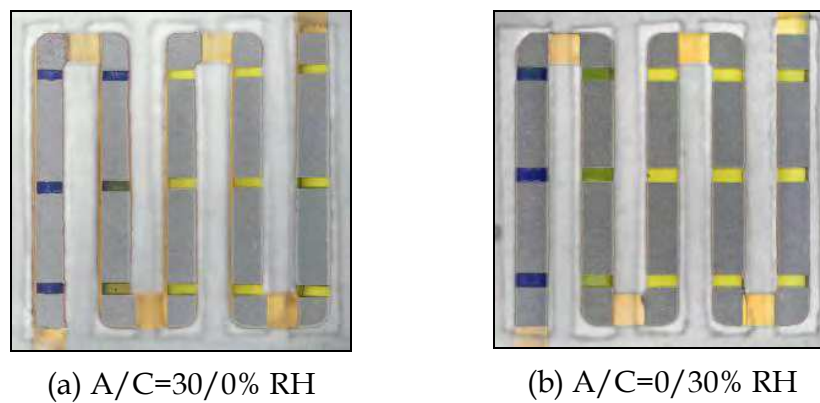

(a) A/C=30/0% RH   (b) A/C=0/30% RH

Fig. 20. Discoloration images of WSP in the anode channel for two different humidification conditions (Anode/Cathode(A/C)=30/0%, 0/30% RH) at high current density of 0.3 A/cm²
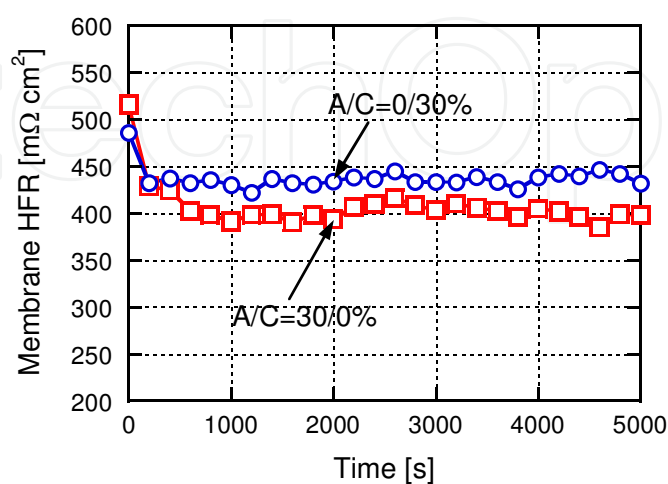

Fig. 21. Membrane HFRs for different humidification conditions (A/C=30/0%, 0/30% RH) at high current density of 0.3 A/cm²

Figure 21 shows the membrane HFR during high current density operation at two humidification conditions. Since the membrane dehydration proceeds with an increase in current density, the membrane resistance at 0.3 A/cm² becomes higher than that at 0.1 A/cm² provided in Figure 19. In addition, during high current density operation, the membrane HFR for the anode humidification case of A/C=30/0% is lower than that for the cathode humidification of A/C=0/30%. It should be noted that humidification of anode inlet gas alleviates membrane dryout and improves cell performance under low-humidity conditions.

6. Conclusions

In this chapter, three novel diagnostic tools for investigating the water transport phenomena inside a PEFC were developed. These measurement techniques can provide important information about water transport in fuel cell without the use of specialized equipments such as neutron radiography and X-ray computed tomography. In the first part of this chapter, the experimental method for estimating the liquid water content in the cathode GDE of a PEFC was presented based on the weight measurement. Furthermore, the optical visualization tool to explore the liquid water behavior was provided using a transparent fuel cell, and the impacts of current density and GDL thickness on the water transport in the cathode electrode were discussed. In the second part, the liquid water accumulation at the interface between the cathode CL and GDL was quantitatively measured using near-infrared reflectance spectroscopy (NIRS). The results showed that hydrophobic treatment of GDL is effective in alleviating water flooding at cathode CL|GDL interface. In addition, liquid water film at cathode interface is not formed at all by microporous layer (MPL) addition. The third part introduced the unique imaging technique to observe the water distribution in the anode flow field of a low-humidity PEFC using water sensitive paper (WSP). It was found that humidification of anode inlet gas prevents membrane dryout and enhances fuel cell power effectively under low-humidity conditions.

7. Acknowledgements

8. References

Bellows, R.J.; Lin, M.Y.; Arif, M.; Thompson, A.K. & Jacobson, D. (1999). Neutron Imaging Technique for In Situ Measurement of Water Transport Gradients within Nafion in Polymer Electrolyte Fuel Cells, *Journal of the Electrochemical Society*, Vol.146, No.3, (March 1999), pp. 1099-1103, ISSN 0013-4651

Boillat, P.; Kramer, D.; Seyfang, B.C.; Frei, G.; Lehmann, E.; Scherer, G.G.; Wokaun, A.; Ichikawa, Y.; Tasaki, Y. & Shinohara, K. (2008). In situ observation of the water distribution across a PEFC using high resolution neutron radiography, *Electrochemistry Communications*, Vol.10, (April 2008), pp. 546-550, ISSN 1388-2481

Curcio, J.A. & Petty, C.C. (1951). The Near Infrared Absorption Spectrum of Liquid Water, *Journal of The Optical Society of America*, Vol.41, No.5, (February 1951), pp. 302-304, ISSN 1084-7529

Gostick, J.T.; Ioannidis, M.A.; Fowler, M.W. & Pritzker, M.D. (2007). Pore network modeling of fibrous gas diffusion layers for polymer electrolyte membrane fuel cells, *Journal of Power Sources*, Vol.173, (November 2007), pp. 277-290, ISSN 0378-7753

He, W.; Yi, J.S. & Nguyen, T.V. (2000). Two-Phase Flow Model of the Cathode of PEM Fuel Cells Using Interdigitated Flow Fields, *AIChE Journal*, Vol.46, No.10, (October 2000), pp. 2053-2064, ISSN 1547-5905

Hickner, M.A.; Siegel, N.P.; Chen, K.S.; McBrayer, D.N.; Hussey, D.S.; Jacobson, D.L. & Arif, M. (2006). Real-Time Imaging of Liquid Water in an Operating Proton Exchange Membrane Fuel Cell, *Journal of the Electrochemical Society*, Vol.153, No.5, (March 2006), pp. A902-A908, ISSN 0013-4651

Kramer, D.; Zhang, J.; Shimoi, R.; Lehmann, E.; Wokaun, A.; Shinohara, K. & Scherer, G.G. (2005). In situ diagnostic of two-phase flow phenomena in polymer electrolyte fuel cells by neutron imaging, Part A. Experimental, data treatment, and quantification, *Electrochimica Acta*, Vol.50, (April 2005), pp. 2603-2614, ISSN 0013-4686

Lee, S.J.; Lim, N.Y.; Kim, S.; Park, G.G. & Kim, C.S. (2008). X-ray imaging of water distribution in a polymer electrolyte fuel cell, *Journal of Power Sources*, Vol.185, (December 2008), pp. 867-870, ISSN 0378-7753

Litster, S.; Sinton, D. & Djilali, N. (2006). Ex situ visualization of liquid water transport in PEM fuel cell gas diffusion layers, *Journal of Power Sources*, Vol.154, (March 2006), pp. 95-105, ISSN 0378-7753

Nam, J.H. & Kaviany, M. (2003). Effective diffusivity and water-saturation distribution in single- and two-layer PEMFC diffusion medium, *International Journal of Heat and Mass Transfer*, Vol.46, (November 2003), pp. 4595-4611, ISSN 0017-9310

Nam, J.H.; Lee, K.J.; Hwang, G.S.; Kim, C.J. & Kaviany, M. (2009). Microporous layer for water morphology control in PEMFC, *International Journal of Heat and Mass Transfer*, Vol.52, (May 2009), pp. 2779-2791, ISSN 0017-9310

Natarajan, D. & Nguyen, T.V. (2001). A Two-Dimensional, Two-Phase, Multicomponent, Transient Model for the Cathode of a Proton Exchange Membrane Fuel Cell Using Conventional Gas Distributors, *Journal of the Electrochemical Society*, Vol.148, No.12, (November 2001), pp. A1324-A1335, ISSN 0013-4651

Nishida, K.; Yokoi, Y.; Tsushima, S. & Hirai, S. (2009). Measurement of Water Distribution in Anode of Polymer Electrolyte Fuel Cell Under Low Humidity Conditions, *Proceedings of the ASME 2009 Seventh International Fuel Cell Science, Engineering and Technology Conference*, Paper No. FUELCELL2009-85128, ISBN 978-0-7918-4881-4, California, USA, June 8-10, 2009

Nishida, K.; Murakami, T.; Tsushima, S. & Hirai, S. (2010a). Measurement of liquid water content in cathode gas diffusion electrode of polymer electrolyte fuel cell, *Journal of Power Sources*, Vol.195, (June 2010), pp. 3365-3373, ISSN 0378-7753

Nishida, K.; Ishii, M.; Taniguchi, R.; Tsushima, S. & Hirai, S. (2010b). Quantitative Evaluation of Liquid Water at Cathode Interface of Polymer Electrolyte Fuel Cell using Near-Infrared Reflectance Spectroscopy, *Proceedings of the ASME 2010 Eighth International Fuel Cell Science, Engineering and Technology Conference*, Paper No. FUELCELL2010-33226, ISBN 978-0-7918-4404-5, New York, USA, June 14-16, 2010

Pasaogullari, U. & Wang, C.Y. (2004a). Liquid Water Transport in Gas Diffusion Layer of Polymer Electrolyte Fuel Cells, *Journal of the Electrochemical Society*, Vol.151, No.3, (February 2004), pp. A399-A406, ISSN 0013-4651

Pasaogullari, U. & Wang, C.Y. (2004b). Two-phase transport and the role of micro-porous layer in polymer electrolyte fuel cells, *Electrochimica Acta*, Vol.49, (October 2004), pp. 4359-4369, ISSN 0013-4686

Rebai, M. & Prat, M. (2009). Scale effect and two-phase flow in a thin hydrophobic porous layer. Application to water transport in gas diffusion layers of proton exchange membrane fuel cells, *Journal of Power Sources*, Vol.192, (July 2009), pp. 534-543, ISSN 0378-7753

Sasabe, T.; Tsushima, S. & Hirai, S. (2010). In-situ visualization of liquid water in an operating PEMFC by soft X-ray radiography, *International Journal of Hydrogen Energy*, Vol.35, (October 2010), pp. 11119-11128, ISSN 0360-3199

Satija, R.; Jacobson, D.L.; Arif, M. & Werner, S.A. (2004). In situ neutron imaging technique for evaluation of water management systems in operating PEM fuel cells, *Journal of Power Sources*, Vol.129, (April 2004), pp. 238-245, ISSN 0378-7753

Sinha, P.K.; Halleck, P. & Wang, C.Y. (2006). Quantification of Liquid Water Saturation in a PEM Fuel Cell Diffusion Medium Using X-ray Microtomography, *Electrochemical and Solid-State Letters*, Vol.9, No.7, (May 2006), pp. A344-A348, ISSN 1099-0062

Sinha, P.K. & Wang, C.Y. (2007). Pore-network modeling of liquid water transport in gas diffusion layer of a polymer electrolyte fuel cell, *Electrochimica Acta*, Vol.52, (November 2007), pp. 7936-7945, ISSN 0013-4686

Sinha, P.K. & Wang, C.Y. (2008). Liquid water transport in a mixed-wet gas diffusion layer of a polymer electrolyte fuel cell, *Chemical Engineering Science*, Vol.63, (February 2008), pp. 1081-1091, ISSN 0009-2509

Springer, T.E.; Zawodzinski, T.A. & Gottesfeld, S. (1991). Polymer Electrolyte Fuel Cell Model, *Journal of the Electrochemical Society*, Vol.138, No.8, (August 1991), pp. 2334-2342, ISSN 0013-4651

Tsushima, S.; Teranishi, K. & Hirai, S. (2004). Magnetic Resonance Imaging of the Water Distribution within a Polymer Electrolyte Membrane in Fuel Cells, *Electrochemical and Solid-State Letters*, Vol.7, No.9, (July 2004), pp. A269-A272, ISSN 1099-0062

Tüber, K.; Pócza, D. & Hebling, C. (2003). Visualization of water buildup in the cathode of a transparent PEM fuel cell, *Journal of Power Sources*, Vol.124, (November 2003), pp. 403-414, ISSN 0378-7753

Turhan, A.; Heller, K.; Brenizer, J.S. & Mench, M.M. (2006). Quantification of liquid water accumulation and distribution in a polymer electrolyte fuel cell using neutron imaging, *Journal of Power Sources*, Vol.160, (October 2006), pp. 1195-1203, ISSN 0378-7753

Wang, Z.H.; Wang, C.Y. & Chen, K.S. (2001). Two-phase flow and transport in the air cathode of proton exchange membrane fuel cells, *Journal of Power Sources*, Vol.94, (February 2001), pp. 40-50, ISSN 0378-7753

Yang, X.G.; Zhang, F.Y.; Lubawy, A.L. & Wang, C.Y. (2004). Visualization of Liquid Water Transport in a PEFC, *Electrochemical and Solid-State Letters*, Vol.7, No.11, (October 2004), pp. A408-A411, ISSN 1099-0062

Yoshizawa, K.; Ikezoe, K.; Tasaki, Y.; Kramer, D.; Lehmann, E. & Scherer, G.G. (2008). Analysis of Gas Diffusion Layer and Flow-Field Design in a PEMFC Using Neutron Radiography, *Journal of the Electrochemical Society*, Vol.155, No.3, (January 2008), pp. B223-B227, ISSN 0013-4651

Zhang, F.Y.; Yang, X.G. & Wang, C.Y. (2006). Liquid Water Removal from a Polymer Electrolyte Fuel Cell, *Journal of the Electrochemical Society*, Vol.153, No.2, (December 2005), pp. A225-A232, ISSN 0013-4651

Zhang, J.; Kramer, D.; Shimoi, R.; Ono, Y.; Lehmann, E.; Wokaun, A.; Shinohara, K. & Scherer, G.G. (2006). In situ diagnostic of two-phase flow phenomena in polymer electrolyte fuel cells by neutron imaging, Part B. Material variations, *Electrochimica Acta*, Vol.51, (March 2006), pp. 2715-2727, ISSN 0013-4686

Recent Trend in Electrochemical Science and Technology
Edited by Dr. Ujjal Kumar Sur

This book titled "Recent Trend in Electrochemical Science and Technology" contains a selection of chapters focused on advanced methods used in the research area of electrochemical science and technologies; descriptions of electrochemical systems; processing of novel materials and mechanisms relevant for their operation. This book provides an overview on some of the recent development in electrochemical science and technology. Particular emphasis is given both to the theoretical and the experimental aspect of modern electrochemistry. Since it was impossible to cover the rich diversity of electrochemical techniques and applications in a single issue, the focus is on the recent trends and achievements related to electrochemical science and technology.

How to reference

In order to correctly reference this scholarly work, feel free to copy and paste the following:

Kosuke Nishida, Shohji Tsushima and Shuichiro Hirai (2012). Water Management and Experimental Diagnostics in Polymer Electrolyte Fuel Cell, Recent Trend in Electrochemical Science and Technology, Dr. Ujjal Kumar Sur (Ed.), ISBN: 978-953-307-830-4, InTech, Available from:
http://www.intechopen.com/books/recent-trend-in-electrochemical-science-and-technology/water-management-and-experimental-diagnostics-in-polymer-electrolyte-fuel-cell

INTECH
open science | open minds